scientific reports

Check for updates

OPEN

Neurodynamic robust adaptive UWB localization algorithm with NLOS mitigation

Yanxu Liu[1✉], Enwen Hu[2], Yudong Chen[1] & Changyou Guo[1]

For the robust localization in mixed line-of-sight (LOS) and non-line-of-sight (NLOS) indoor environments, we proposed a max-min optimization estimator from a measurement model and introduced an adaptive loss function to optimize the estimation. However, this estimator is highly nonconvex leading to difficulties in solving it directly. We employed the neurodynamic to solve it. In addition, we checked the local equilibrium stability of the corresponding projective neural network model. The proposed algorithm does not require any prerequisites compared to existing algorithms, which either require knowledge of the magnitude of the NLOS bias or a priori distinction between LOS and NLOS. We proposed an adaptive distance error upper bound method to improve the accuracy of localization model. Tested in representative numerical simulation and real environments, our proposed robust adaptive positioning algorithm outperforms existing methods in terms of localization accuracy and robustness, especially in severe NLOS environments.

In the increasingly digital and intelligent world of today, localization technology has become critical[1,2]. It plays a key role in variety of areas, such as helping people navigate through large buildings, improving the efficiency of traffic management, enhancing personal safety, and providing support in the Internet of Things(IoTs) and smart homes[3–5]. Highly accurate and robust positioning technology has become one of the most important prerequisites to support various applications.

Although global satellite navigation systems are widely used in outdoor environments, it is difficult to achieve positioning in heavily occluded indoor environments due to the weak signal strength of navigation satellite signals, which makes it difficult to penetrate buildings[6]. Various indoor positioning technologies such as Wi-Fi and Bluetooth positioning have made great strides in the last few decades[7,8] However, as the requirements for positioning accuracy and reliability have increased, the traditional technology is limited by positioning technology itself and is difficult to meet.

Compared to traditional technologies, the Ultra-Wideband (UWB) has advantages of low power consumption, high distance measurement accuracy, low cost, etc[9]. It can be widely used for positioning in indoor, urban and industrial environments capable of realizing high-precision positioning[10].

The UWB localization algorithm is based on relative distance measurements obtained from the timing and signal characteristics of radio signals, which are further calculated to determine positioning of the node. Compared to time-difference-of-arrival (TDOA), angle of arrival (AOA) and received signal strength indicator (RSSI) localization techniques, time-of-arrival (TOA) has a large advantage in terms of accuracy and computational overhead. Typically studies of TOA-based techniques assume a LOS environment[11]. But normally in indoor scenarios, UWB signals suffer from NLOS, multipath, and other interferences, resulting in large deviations in the information measured by the signals, which leads to a sharp drop in positioning accuracy, or even the inability.

For localization methods with NLOS mitigation, existing studies are categorized into localization methods based on weighted least squares, filtering, machine learning, to name a few. Localization methods based on weighted least squares utilize all available UWB measurements for position, with each measurement having its own weight. For LOS measurements with a larger weight and NLOS measurements have a smaller weight, which reduces the impact of NLOS errors on positioning. Under the a priori assumption of NLOS measurements, a least squares algorithm was used to perform a global search, and then the optimal initial value was obtained by threshold screening and weight calculation, which improved localization accuracy by 63% compared to least

[1]College of Computer and Information, Dezhou University, Dezhou 253023, China. [2]School of Electronic Engineering, Beijing University of Posts and Telecommunications, Beijing 100876, China. ✉email: liuyanxu@dzu.edu.cn

squares algorithm[12]. For the mixed LOS/NLOS environment with unknown anomaly variance, a weighted least squares method based on Hampel and jump filters is proposed to estimate positioning and reduce the impact of NLOS error on localization[13]. To mitigate NLOS errors of localization algorithms based on weighted least squares, the value of weights must be considered. As a result, algorithm performance relies on feature recognition of measurement, leading to limited localization accuracy in real-world.

Among the filtering-based localization methods, Yang et al. proposed a localization method based on particle filtering, which is filtered twice in order to reduce the effect of NLOS errors and improve localization accuracy[14]. The algorithm can handle nonlinear and non-Gaussian system model, which requires fewer assumptions of the model and increase the number of particles to reduce NLOS error. However, computational complexity is high, due to large number of particles to be processed. In addition, the calculation results of particle filtering algorithm have a certain degree of uncertainty because of introduction of randomness. Therefore, it is difficult to ensure the reliability of localization when applied in a real.

Localization methods based on filtering and weighted least squares need to first determine the NLOS state of ToA measurements before localization, which is computationally expensive and suffers from misidentification, whereas machine have been widely applied for LOS/NLOS identification[15,16]. There are already several machine learning-based approaches that can directly achieve robust estimation of the localization state without need for a known NLOS state[17]. A maximum likelihood (ML) position estimator is derived from measurement model, and localization problem is then transformed into a generalized trust domain subproblem (GTRS)[18].

Thereafter, localization problem is reshaped into an optimized form using semidefinite relaxation (SDR) or second-order cone relaxation (SOCR) as well as regularized total least square semidefinite program (RTLS-SDP)[11], new robust semidefinite programming method (RDSP-New)[19], semidefinite programming (SDP)[20]. Another idea is to improve position estimator by constructing a robust localization optimization problem, based on maximum correntropy criterion (MCC)[21], which does not require any a priori assumptions and can achieve robust estimation under NLOS[22]. However, these methods cannot eliminate the bias in TOA measurements and cannot adaptively change the positioning model according to the NLOS environment, leading to a decrease in localization accuracy.

The primary contribution of this paper is introduction of a robust adaptive localization algorithm for indoor UWB localization, based on neurodynamic principles. This contribution is characterized by two key aspects of adaptation robust: the first one is adaptation robust during localization solving process, while the second focuses on adaptation of localization model itself. By incorporating an adaptive robust function, our method advances existing localization model, resulting in development of a robust adaptive localization model. This approach distinguishes itself from traditional methods, such as MCC, by its ability to dynamically adapt based on the number of iterations, thereby providing enhanced flexibility and robustness across various localization scenarios. We apply the neurodynamic to effectively solve the localization model based on adaptive robust optimization problem and analyze the local stability of localization solution. Our localization model is different from other methods in that it can estimate the distance error bounds and adjust the localization model to achieve higher accuracy.

UWB adaptive robust localization model
The measurement model
Consider a 2D indoor localization scenario containing N UWB anchor and one unknown nodes. The positioning of i-th anchor node is denoted as $x_i \in \mathbb{R}^2$ and positioning of unknown node is represented as $x \in \mathbb{R}^2$.

The x is calculated by the relative distances to the anchor nodes, and d_i is the Euclidean distance between unknown and i-th anchor node, defined as:

$$d_i = \|x - x_i\|_2 , i = 1, 2, \ldots, N. \tag{1}$$

where $\| \cdot \|_2$ denotes a L2 norm. Considering the indoor NLOS error and observation noise, the observation model of relative distance can be expressed as:

$$r_i = d_i + n_i + q_i, i = 1, 2, \ldots, N. \tag{2}$$

where r_i denotes relative distance observation, n_i is UWB measurement noise, which satisfies the Gaussian distribution $\mathbb{N}(0, \sigma_i)$. q_i is NLOS measurement error, when $q_i = 0$ denotes a LOS condition.

Introduce adaptive robust loss function
The adaptive robust loss function is[23]:

$$f(L, \alpha, c) = \frac{|\alpha - 2|}{\alpha} \left(\left(\frac{(L/c)^2}{|\alpha - 2|} + 1 \right)^2 - 1 \right). \tag{3}$$

where $c > 0$ is a scale parameter that determines the degree of bending near $L = 0$, and L is the original loss function. α is a hyperparameter that controls the solution robustness of optimization problem, and different values of α, the loss function can be expressed as follows:

$$f\left(L,\alpha,c\right) = \begin{cases} 1 - e^{-\frac{1}{2}\left(\frac{L}{c}\right)^2} & if\ \alpha = -\infty \\ \log\left(\frac{1}{2}\left(\frac{L}{c}\right)^2 + 1\right) & if\ \alpha = 0 \\ \frac{1}{2}\left(\frac{L}{c}\right)^2 & if\ \alpha = 2 \\ \frac{|\alpha-2|}{\alpha}\left(\left(\frac{(L/c)^2}{|\alpha-2|}+1\right)^2 - 1\right) & otherwise \end{cases} \quad . \tag{4}$$

The adaptive loss function with $\alpha = 2$ is equivalent to L2 loss, while using $\alpha = 1$ is a smoothed form of L1 loss, Charbonnier loss or L1–L2 loss. When $\alpha = -\infty$, it approaches local mode finding. The α can be thought of as a smooth interpolation between these three averages during the estimation process, the robustness of the loss function to be automatically adapted during optimization of localization process, thus improving the localization performance without the need for any manual parameter tuning.

Problem formulation
Assuming UWB indoor localization without any NLOS a priori information. And according to Eq. (2), the L2 optimization problem for indoor UWB localization can be established as

$$\min_{x} \max_{\in} \sum_{i=1}^{N} \left(r_i - d_i - \in_i\right)^2 \quad . \tag{5}$$
$$s.t.0_N \leq \in \leq \delta$$

where $\in = [\in_1, \ldots, \in_N]^T$, $\delta = [\delta_1, \ldots, \delta_N]^T$. 0_N denotes an N-dimensional column vector with all elements 0, $\epsilon \leq \delta$ means $\epsilon_i \leq \delta_i$ with $i = 1, 2, \ldots, N$. $\epsilon_i = n_i + q_i$ is distance error between unknown and i-th anchor node. δ_i is the upper bound of ranging error ϵ_i, which is usually unknown in real world, and setting the value of δ_i too large or too small will degrade the accuracy. Because of the continuity of motion trajectory, the upper bound of measurements varies less in a short period of time, for this reason, we proposed an adaptive robust (AR) method that approximates the error upper bound by an estimate of ϵ_i as

$$\delta_{i,t} = \beta \cdot \max\left\{\in_{1,t-1}, \ldots, \in_{i,t-1}\right\}, i = 1, \ldots, N. \tag{6}$$

where $\beta \geq 1$ is the amplification factor, which ensures that avoiding the $\delta_{i,t}$ too small when distance error become large. For simplicity, t will be omitted. In order to solve optimization problem (5), we transform it into an equivalent as

$$\min_{x,\in} \gamma$$
$$s.t.\gamma \geq \sum_{i=1}^{N}\left(r_i - d_i - \in_i\right)^2 \quad . \tag{7}$$
$$0_N \leq \in \leq \delta$$

NLOS leads to UWB relative distance measurements with large measurement errors ϵ_i. Therefore, the L2 loss function degrades accuracy and reliability of indoor positioning. For this reason, from the idea of robust learning in machine learning, combined with the adaptive robust loss function in Eq. (3). Then, the adaptive robust optimization function for indoor UWB positioning is

$$\min_{x,e_i} \gamma$$
$$s.t.\gamma \geq f\left(L,\alpha,c\right) \quad . \tag{8}$$
$$0_N \leq \in \leq \delta$$

where L is denoted as

$$L = \sum_{i=1}^{N}\left(r_i - d_i - \in_i\right)^2 . \tag{9}$$

The α and c affect robustness and convergence speed of loss function, and $f\left(L,\alpha,c\right)$ is monotonically increasing with respect to α. By gradually decreasing α, we can avoid optimization process from getting stuck in local optima, thereby enhancing the robustness of the position coordinate estimation. c determines the gradient of loss function f in the neighborhood of optimal solution. When $|L| < c$, the gradient value $\frac{\partial f}{\partial L}$ is linearly proportional to L for any parameter α, and can converge to optimal solution quickly and precisely. Therefore, we draw on α and c adaptive methods in the reference[23] to establish robust adaptive factors for UWB indoor localization. α and c is

$$\alpha_k = \left(\alpha_{max} - \alpha_{min}\right) S\left(\alpha_{k-1}\right) + \alpha_{min}$$
$$c_k = \psi\left(c_{k-1}\right) + c_{min} \quad . \tag{10}$$
$$\alpha_{min} = 0, \alpha_{max} = 3, c_{min} = 10^{-8}$$

where α_k and c_k denote the hyperparameters of loss function f for the k-th iteration operation, respectively. $S(\cdot)$ and $\psi(\cdot)$ are the sigmoid and softplus functions, respectively, defined as

$$
\begin{aligned}
S(x) &= \frac{1}{1+e^{-x}} c_k \\
\psi(x) &= \log(1+e^x)
\end{aligned}
\tag{11}
$$

Neurodynamic robust localization algorithm
Consider the nonconvex nonlinear optimization problem with inequality constraints

$$
\begin{aligned}
&\min_z f(z) \\
&s.t. g(z) \le 0_M
\end{aligned}
\tag{12}
$$

where $g(z) = [g_1(z), g_2(z), \ldots, g_M(z)]^T \in \mathbb{R}^M$ is a vector function in dimension M, and $f, g_1, g_2 \ldots, g_m$ are a quadratically continuous differentiable function. $0_M \in \mathbb{R}^M$ is an M-dimensional zero vector. The Lagrangian function of optimization problem Eq. (12) is:

$$
\mathcal{L}(z, u) = f(z) + u^T g(z).
\tag{13}
$$

where $u = [u_1, u_2, \ldots, u_M]^T \in \mathbb{R}^M$ is a vector of Lagrange multipliers. The necessary condition for optimal solution is then to satisfy the KKT condition as

$$
\begin{aligned}
&\nabla_z \mathcal{L}(z^*, u^*) = \nabla_z f(z^*) + u^{*T} \nabla_z g(z^*) = 0 \\
&g_i(z^*) \le 0 \\
&u_i^{*T} g(z_i^*) = 0 \\
&u_i^* \ge 0
\end{aligned}
\tag{14}
$$

z^* is the locally optimal solution to optimization problem Eq. (12). The projective form of augmented Lagrangian function can be obtained as

$$
\begin{aligned}
&\nabla_z \mathcal{L}_\rho(z^*, u^*) = 0 \\
&[u_i^* + g_i(z^*)]^+ - u_i^* = 0
\end{aligned}
\tag{15}
$$

where $\mathcal{L}_\rho(z, u) = \mathcal{L}(z, u) + \frac{\rho}{2} \sum_{i=1}^{M} [u_i g_i(z)]^2$ is augmented Lagrangian function, $\rho > 0$ is augmented Lagrange parameter. The operator $[\cdot]^+ = max(\cdot, 0)$ represents the primal feasibility, pairwise feasibility, and complementarity conditions of the inequality constraints equivalently in projective form.

Based on Eq. (15), KKT points of optimization problem Eq. (12) can be calculated by projection neural network (PNN). Therefore, the localization problem is formulated using a recurrent neural network model[24,25] and is represented as:

$$
\begin{aligned}
&\frac{d\omega}{dt} = T(\omega) = \begin{bmatrix} -\nabla_z \mathcal{L}_\rho(\omega) \\ [u + g(z)]^+ - u \end{bmatrix} \\
&\nabla_z \mathcal{L}_\rho(\omega) = \nabla_z \mathcal{L}(\omega) + \rho \sum_{i=1}^{M} u_i^2 g_i(z) \nabla_z g_i(z)
\end{aligned}
\tag{16}
$$

where $\omega = [z^T, u^T]^T$. Figure 1 shows how recurrent neural network based on neurodynamic model described by Eq. (16) has been implemented in hardware.

Next, recurrent neural network will be used to solve optimization problem Eq. (8), which can be transformed into

$$
\begin{aligned}
&\min_{x, \in} \gamma \\
&s.t. \frac{|\alpha-2|}{\alpha} \left(\left(\frac{(L/c)^2}{|\alpha-2|} + 1 \right)^2 - 1 \right) - \gamma \le 0 \\
&\in - \delta \le 0_N \\
&- \in \le 0_N
\end{aligned}
\tag{17}
$$

Comparing Eq. (17) with optimization problem Eq. (13) can be obtained

$$
\begin{aligned}
&z = \begin{bmatrix} x^T, \in^T, \gamma \end{bmatrix}^T \\
&f(z) = \gamma \\
&g(z) = \begin{bmatrix} \frac{|\alpha-2|}{\alpha} \left(\left(\frac{(L/c)^2}{|\alpha-2|} + 1 \right)^2 - 1 \right) \\ -\gamma \\ (\in - \delta)^T \\ - \in^T \end{bmatrix} \\
&M = 2N + 2
\end{aligned}
\tag{18}
$$
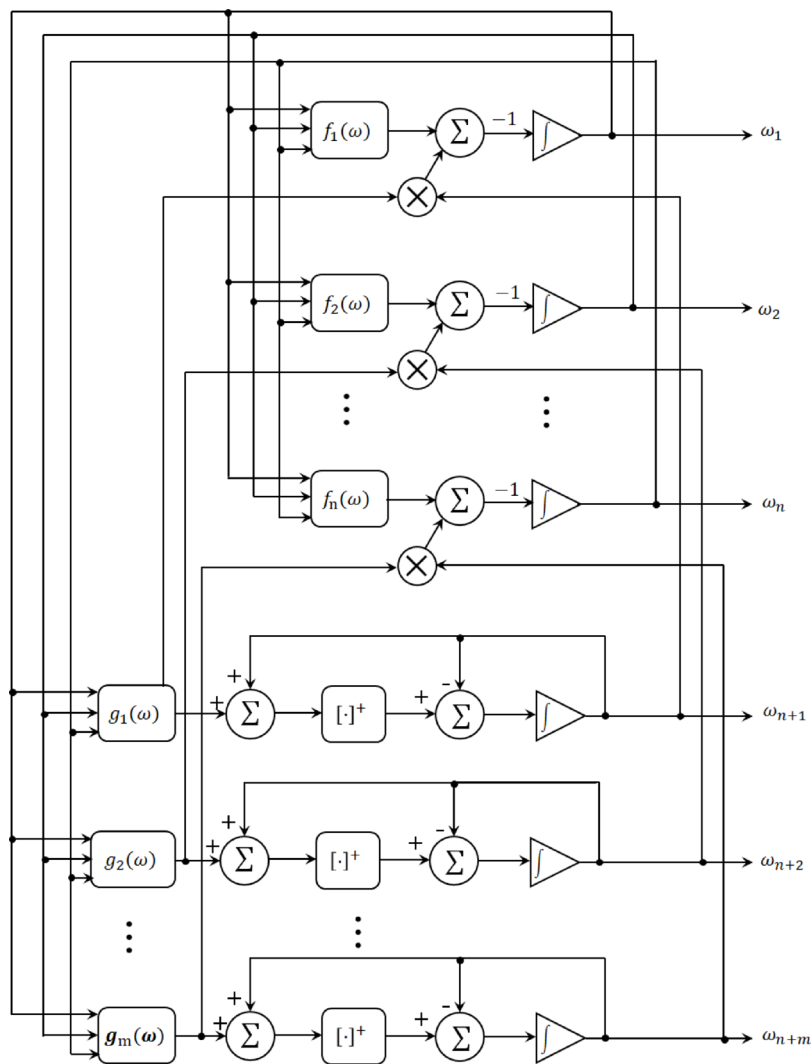
Fig. 1. Structure of recursive neural network.

The $\mathcal{L}_p(z, u)$ is

$$\mathcal{L}_p(z, u) = \gamma + u^T g(z) \ . \tag{19}$$

Several relatively complex gradient calculations in Eq. (16) are

$$
\begin{aligned}
\frac{\partial \mathcal{L}_p(z,u)}{\partial x} &= \frac{|\alpha - 2|u_1}{\alpha}\left(\frac{\left(\frac{1}{c}\cdot\frac{\partial L}{\partial x}\right)^2}{|\alpha - 2|} + 1\right)^2 \\
\frac{\partial L}{\partial x} &= \sum_{i=1}^{N}\frac{\partial(r_i - d_i - \in_i)^2}{\partial x} = -2\sum_{i=1}^{N}\frac{\partial d_i}{\partial x}(r_i - d_i - \in_i) \\
\frac{\partial d_i}{\partial x} &= \frac{\partial\|x - x_i\|_2}{\partial x} = \frac{x - x_i}{d_i} \\
\frac{\partial \mathcal{L}_p(z,u)}{\partial \in} &= u_{3:N+2}^T - u_{N+3:2N+2}^T \\
\frac{\partial \mathcal{L}_p(z,u)}{\partial \gamma} &= 1 - u_2
\end{aligned}
\tag{20}
$$

Stability and convergence
In this section, we discuss two important properties of neural network formulation Eq. (16), stability and convergence.

Theorem 1 *If $\omega^* = \left[z^T, u^T\right]^T$ is the equilibrium point of neural network in Eq. (16), then ω^* is the KKT point of optimization problem in Eq. (12).*

Proof If $\omega^* = \left[z^T, u^T \right]^T$ is equilibrium point of neural network Eq. (16), then there is.

$$\frac{d\omega^*}{dt} = \frac{dz^*}{dt} = \frac{du^*}{dt} = 0 \quad . \tag{21}$$

It is equivalent to

$$\begin{aligned} \nabla_z \mathcal{L}_\rho \left(\omega^* \right) &= 0 \\ \left[u^* + g \left(z^* \right) \right]^+ &= u^* \end{aligned} \quad . \tag{22}$$

If and only if $g_i \left(z^* \right) \le 0, u_i^{*T} g \left(z_i^* \right) = 0, u_i^* \ge 0$, satisfies $\left[u^* + g \left(z^* \right) \right]^+ = u^*$. Substituting into Eq. (22) yields $\nabla_z \mathcal{L} \left(\omega^* \right) = \nabla_z \mathcal{L}_\rho \left(\omega^* \right) = 0$. Thus ω^* is equilibrium point of neural network and is also KKT point.

Theorem 2 *The neurodynamic model Eq.* (16) *is asymptotically stable at KKT point* ω^*, *where* z_i^* *is a strict local minimum of optimization problem.*

Proof Consider the following Lyapunov equation is.

$$V \left(\omega \right) = -F \left(\omega \right) T \left(\omega \right) - \frac{1}{2} \left\| T \left(\omega \right) \right\|_2^2 + \frac{1}{2} \left\| \omega - \omega^* \right\|_2^2 \quad . \tag{23}$$

where

$$F \left(\omega \right) = \left[\begin{array}{c} \nabla_z \mathcal{L}_\rho \left(\omega \right) \\ -g \left(z \right) \end{array} \right] . \tag{24}$$

According to Theorem 2 in reference [26], if $\frac{\widehat{d\omega}}{dt} = 0$, then there is $\frac{dV(\widehat{\omega})}{dt} = 0$. According to $\frac{dV}{dt} = 0$, we have

$$\begin{aligned} F \left(\hat{\omega} \right) \left(\hat{\omega} - \omega^* \right) &= 0 \\ T \left(\hat{\omega} \right)^T \nabla F \left(\hat{\omega} \right) T \left(\hat{\omega} \right) &= 0 \\ \left(F \left(\hat{\omega} \right) - F \left(\omega^* \right) \right)^T \left(\hat{\omega} - \omega^* \right) &= 0 \\ \frac{dV(\hat{\omega})}{dt} &\le - \left(F \left(\hat{\omega} \right) - F \left(\omega^* \right) \right)^T \left(\hat{\omega} - \omega^* \right) \end{aligned} \quad . \tag{25}$$

where $\hat{\omega}$ is denoted as neighbor of ω^*, according to Eq. (25) there is

$$\begin{aligned} \hat{z} &= x^* \\ g \left(\hat{\omega} \right)^T \left(\hat{u} - u^* \right) &= 0 \end{aligned} \quad . \tag{26}$$

Therefore, we can obtain

$$\begin{aligned} g \left(\hat{\omega} \right)^T \hat{u} &= g \left(\omega^* \right)^T u^* \\ \left[u^* + g \left(\omega^* \right)^T \right]^+ &= u^* \end{aligned} \quad . \tag{27}$$

$\frac{d\omega^*}{dt} = 0$ means that ω^* is equilibrium point of neurodynamic model Eq. (16), and according to Theorem 1, ω^* is also a KKT point. Thus ω^* is asymptotically stable and is a strict local minimum.

Complexity analysis
Using Horner's scheme[27], the evaluation of a polynomial with fixed-size coefficients of degree n can be performed in $O(n)$ time. Considering the polynomial evaluation as the operation in each iteration of Eq. (16) that dictates the computational complexity, it is straightforward to deduce that the dominant complexity of the proposed method (AR-PNN) is $O(N_{PNN} \cdot N^2)$. The computational complexity of the algorithms considered, such as SR-MCC[21], MCC-PNN[22], RDSP-New[19], RTLS-SDP[11] and AR-PNN, is summarized in Table 1. Where N_{PNN} denotes the number of iterations taken in discretely realizing the PNN, K is the number of steps taken by bisection search, and N_{HQ} denotes the number of half-quadratic (HQ) iterations[21].

Algorithm	Description	Complexity
SR-MCC	The MCC-based robust method[21]	$O(N_{HQ} K N)$
MCC-PNN	The robust MCC-PNN method[22]	$O(N_{PNN} \cdot N^2)$
RDSP-New	The robust RDSP-New method[19]	$O(N^{6.5})$
RTLS-SDP	The robust RTLS SDP method[11]	$2 \times O(N^{6.5})$
AR-PNN	The proposed method	$O(N_{PNN} \cdot N^2)$

Table 1. Summary of the considered algorithm.

Numerical results

We first validate the algorithm through numerical simulation and then verify the proposed algorithm through experimental data in real world in the next section. The purpose of the simulation is to verify localization performance and robustness of AR-PNN.

Simulation setup

The simulation in this section is divided into three parts, firstly to verify the adaptive ranging error bound of the proposed algorithm, and then to verify localization accuracy and robustness of AR-PNN under LOS and NLOS environments, respectively. The positioning of 10 anchor and unknown nodes are randomly generated and are localized in a $20m \times 20m$ area. Different parts of simulation have different parameters, specifically in terms of the number of NLOS paths, ranging error variance σ_i, and maximum NLOS error q_m. In each simulation, NLOS paths are randomly assigned, and measurements used by different algorithms remain completely identical. The localization performance is evaluated by the root mean square error (RMSE) and the error cumulative distribution function (CDF).

Distance error upper bound adaptation study

To verify the effectiveness of AR-PNN, we verified ranging error bounds adaption under LOS and NLOS conditions. Evaluate error upper bound performances by averaging error. For visualization, we plotted only the last 100 results. We assume that the NLOS error q_i satisfies a uniform distribution $U(0, q_m)$. $max(\epsilon)$ is maximum measurements error. L_{NLOS} indicates the number of NLOS paths, when $L_{NLOS} = 0$ means in LOS environment. Six different conditions were analyzed, and each condition was tested with 3000 Monte Carlo (MC) simulations. L_{NLOS} NLOS paths are randomly selected. Figure 2 below gives the error upper bounds adaptive under six conditions.

It can be seen that the actual estimates are large in comparison, which is beneficial in the localization model to ensure correctness of localization model Eq. (8). However, it needs to be ensured that error bounds do not deviate too much from actual values, otherwise the problem of large positional estimation errors will occur. The average error between actual and estimated error bound is given in Table 2, and it can be seen that it is basically less than 0.35 m, which ensures positioning estimation performance.

Impact of the ranging noise σ_i in LOS

We evaluate localization performance of AR-PNN, RDSP-New, SR-MCC, RTLS-SDP, and MCC-PNN algorithms under different Gaussian noise σ_i variances in a LOS environment. The positionings of unknown and anchor nodes are randomized at each MC. The TOA measurements follow a Gaussian distribution with standard deviations σ_i ranging from $0.1m$ to $5m$ at 0.1 m intervals. The RMSE for different σ_i were obtained by running 3000 MCs. Figure 3 shows RMSE results of 5 algorithms for different ranging error distributions. AR-PNN has a smaller RMSE than any other algorithm, especially when σ_i is large, the difference is more obvious. Since there are no NLOS paths in Fig. 3, both MCC-PNN and our proposed algorithm have similar formulations for localization optimization function, with the performance difference mainly arising from robust function. In this case, our algorithm can be viewed as an MCC-PNN algorithm with a modified robust function. As seen in Fig. 3, AR-PNN has significant performance improvements when the measurement noise is large, which highlights the impact of the robust function.

Impact of the localization performance in mild, moderate, and severe NLOS environments

Fixing ranging noise to $\sigma_i = 0.1m$, Fig. 4 exhibits relationship between localization performance and maximum NLOS error $q_m \in [1,5]\,m$ for three representative light, medium and heavy NLOS environments. 3000 MCs were run with different environments.

We find that localization performance of algorithms deteriorate gradually with increasing q_m. AR-PNN has least deterioration among all the methods and has better robustness to increasing NLOS errors. Because AR-PNN can adaptively adjust the distance error bounds with a more accurate localization model relative to other algorithms. During the localization process, the adaptive robust loss function can better converge to the vicinity of the best solution, thus providing better scene adaptation and localization performance. This also makes localization performance of all algorithms progressively worse as the number of NLOS paths becomes larger. Nonetheless, especially in severe NLOS environments, AR-PNN has better localization performance and robustness compared to other methods. The same NLOS error distribution in different environments also minimizes the degradation of AR-PNN localization performance in most cases. Therefore, in the mild case of NLOS and errors, the performance and robustness of all localization methods are basically comparable. But in moderate and severe cases, AR-PNN has better localization performance and robustness.

Further analysis reveals that the key advantage of our proposed method lies in its ability to adaptively adjust the upper bound of distance error, which significantly enhances localization accuracy under challenging conditions with many NLOS paths. The robust function plays a crucial role in maintaining stability in the presence of sensor noise under LOS environment (as illustrated in Fig. 3). Its effect is less noticeable when sensor noise is relatively low ($\sigma_i = 0.1m$), as comparison with MCC-PNN, SR-MCC, and RTLS-SDP shows. In this case, impact of different robust functions on performance is minimal. As demonstrated in Fig. 4, when number of NLOS paths increases, performance improvement of our proposed becomes more pronounced. This is due to method's ability to better handle the NLOS distortions, providing a more accurate estimate of unknown node's position. In contrast, robust function mainly addresses performance degradation caused by large observation noise in sensors themselves.
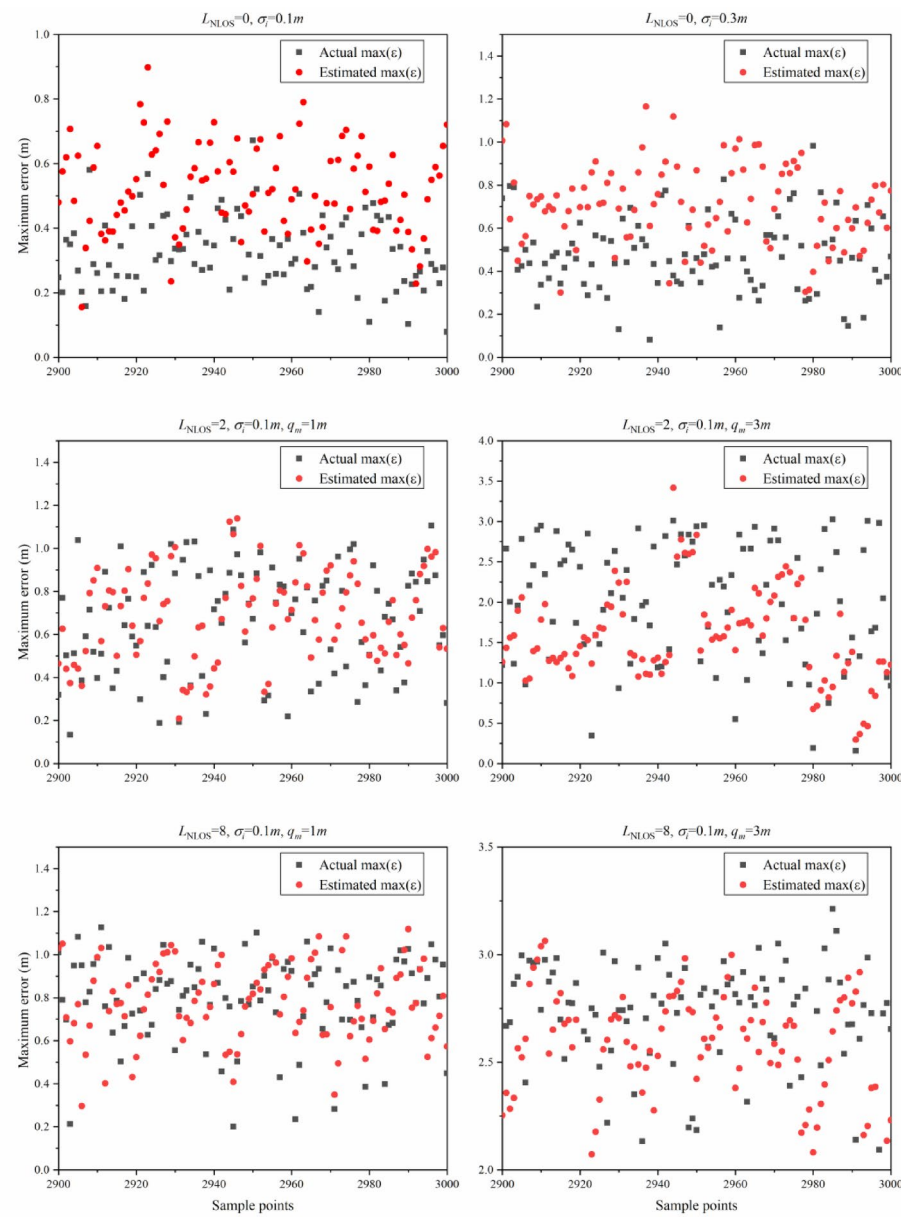
Fig. 2. Dynamic behaviors of $max(\epsilon)$ estimate of time constants for random deployment in NLOS and LOS environments.

L_{NLOS}	σ_i (m)	ϵ_m (m)	Mean error (m)
0	0.1	0	0.14
0	0.3	0	0.26
2	0.1	1	0.22
2	0.1	3	0.35
8	0.1	1	0.20
8	0.1	3	0.29

Table 2. Adaptive mean error of upper bounds.
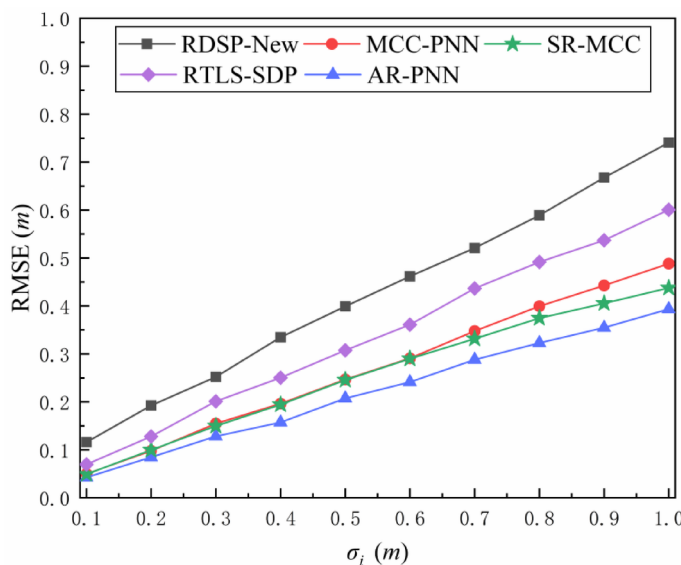
Fig. 3. Comparison of positioning accuracy under different σ_i.

Real world experiments
Dataset detail
In order to validate performance of AR-PNN in real world, we use a UWB localization dataset established by Breger[28]. The positioning system contains 8 UWB anchor and 1 unknown nodes. The distances are realized by DW1000 modules. Use the MQTT and Wi-Fi to collect distance to the laptop.

The localization environment is an indoor apartment, the overall length of the apartment is 12.06 m, width is 9.18 m, the external wall is made of brick structure, and all the internal walls are made of gypsum and thermal insulation materials The environment floor plan and moving trajectory are shown in Fig. 5. The fork symbols denote the positions of the anchor nodes, and position coordinates are shown in Table 3 below.

We first analyzed ranging errors in the real world, and Fig. 6 demonstrates actual ranging errors of all test points. It can be seen that maximum distance error is no more than $4m$. The distribution of distance errors remain roughly constant over short periods of time, but varies to a large extent over long periods of time. Further, we analyzed all distance measurements for each anchor node by box-and-line plots. Figure 7 shows that the mean errors of the measurements for all anchor nodes do not vary much, but the outliers vary considerably. That is to say, it shows the high variability of the distribution of NLOS errors for different anchor nodes, where A1 and A8 have the most severe NLOS errors, and A3 has the lightest impact of distance errors.

Localization performance analysis
To evaluate localization performance in real scenarios, we first analyze trajectories errors. Then we evaluate localization performance by CDF and RMSE.

From Fig. 8, it can be seen that most of trajectory points of AR-PNN are closer to true values than other algorithms. Figure 9 demonstrates that AR-PNN have better performance and robustness among all algorithms. The localization performance was further analyzed by CDF, and it can be seen from Fig. 10. The localization accuracy of MCC-PNN and SR-MCC are close to each other in real world. This may be due to the fact that both methods use the MCC criterion, resulting in similar localization performance and robustness in real-world. Although both AR-PNN and MCC-PNN are based on reflective projection network, the AR-PNN has a more accurate localization model, which makes localization performance better as well. It also shows that the localization loss function is crucial to improve the localization performance and reliability.

Table 4 compares RMSE of different algorithms, and it can be seen that AR-PNN improves significantly compared to other algorithms. The main reason is that compared with other algorithms, AR-PNN takes into account the two main characteristics of the hybrid LOS/NLOS scenarios: small short-term and large long-term variations. By adaptively adjusting localization model, localization model accuracy is improved. Finally, thereby improving the localization performance and robustness.

Conclusion and future work
We proposed a robust adaptive localization method for UWB that does not require any a priori information from NLOS. The UWB distance measurements deteriorate in accuracy due to ambient occlusion and error characteristics change dynamically with environment. Due to nonlinear and nonconvexity of ToA-based localization model, we proposed a neurodynamic approach and verify the local stability conditions for equilibrium of corresponding dynamical system. A robust localization algorithm with adaptive tuning is established from both solution process and localization model. The stability and accuracy of solution is improved by dynamically adjusting loss function in optimization process. On the other hand, measurement error upper bounds are
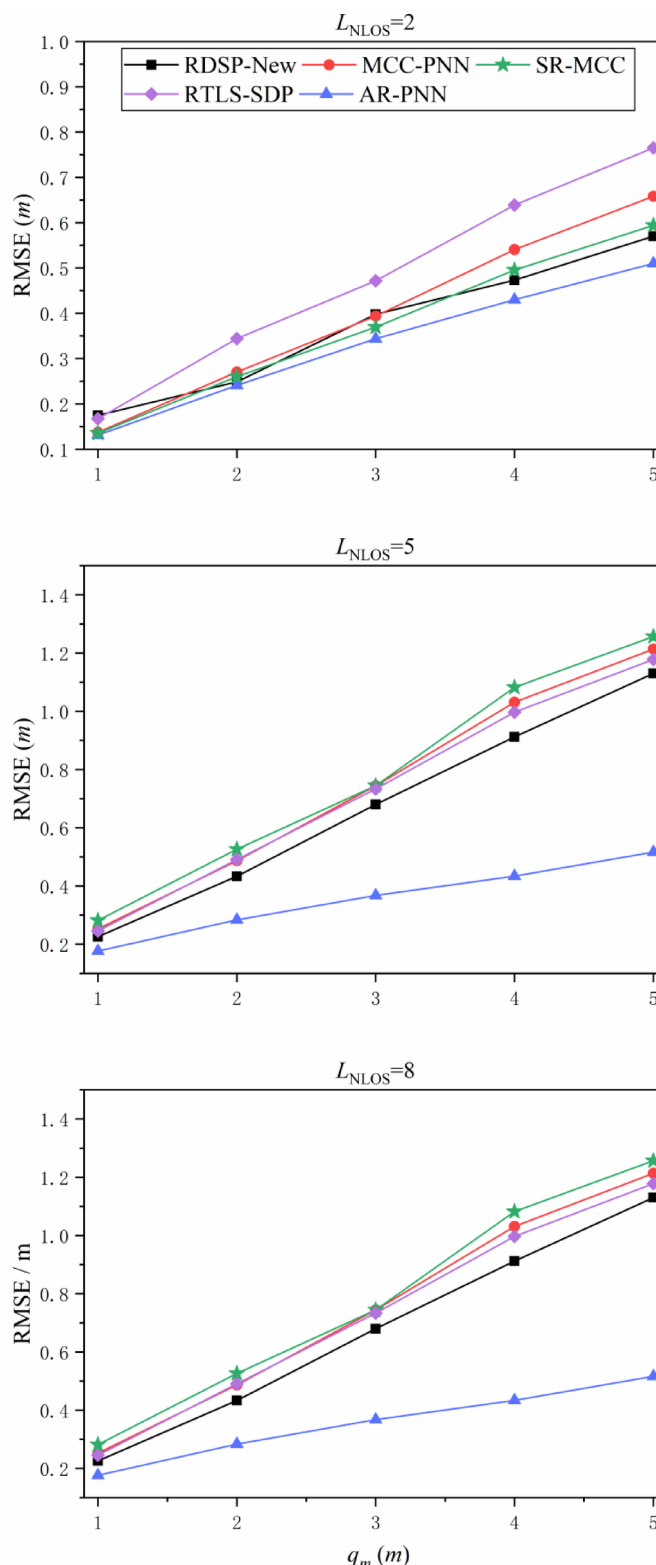
Fig. 4. Comparison of localization accuracy in light, medium and severe NLOS environments.

dynamically estimated for adjusting the localization model. Through these two strategies, the characteristics of small changes in NLOS errors in short time or small area range and large changes in long time are fitted, which makes the localization performance and robustness enhancement significant in the real world.

Our solution can be further applied in the field of autonomous mobile robots. In the future, the algorithm can be improved to fuse sensors such as IMUs and encoders, which can provide high-precision relative localization
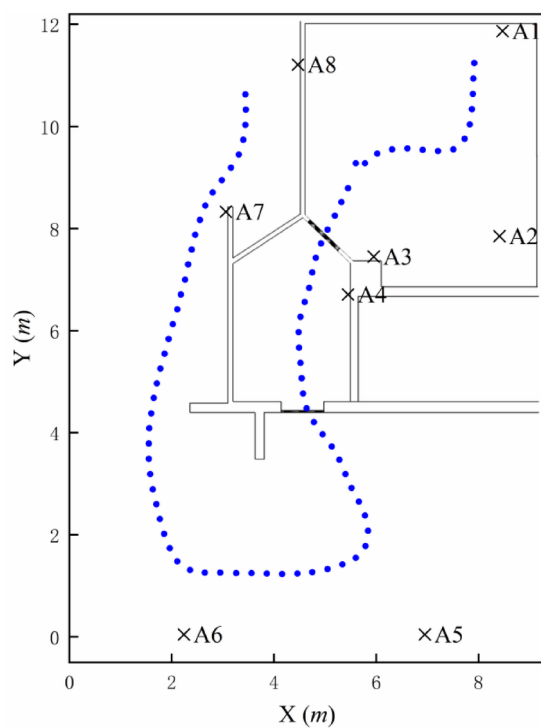
Fig. 5. Indoor localization environments and trajectory.

Anchor node ID	Positioning (m)
A1	(8.47, 11.87)
A2	(8.41, 7.85)
A3	(5.95, 7.45)
A4	(5.45, 6.71)
A5	(6.95, 0.05)
A6	(2.24, 0.05)
A7	(3.06, 8.33)
A8	(4.47, 11.21)

Table 3. UWB anchor node positionings.

in a short period of time, and further improve localization accuracy and robustness when NLOS error changes. On the other hand, neurodynamic approach we adopted can be implemented using neural network-specific hardware, integrated into a single sensor, which can reduce power consumption and expand range of applications.
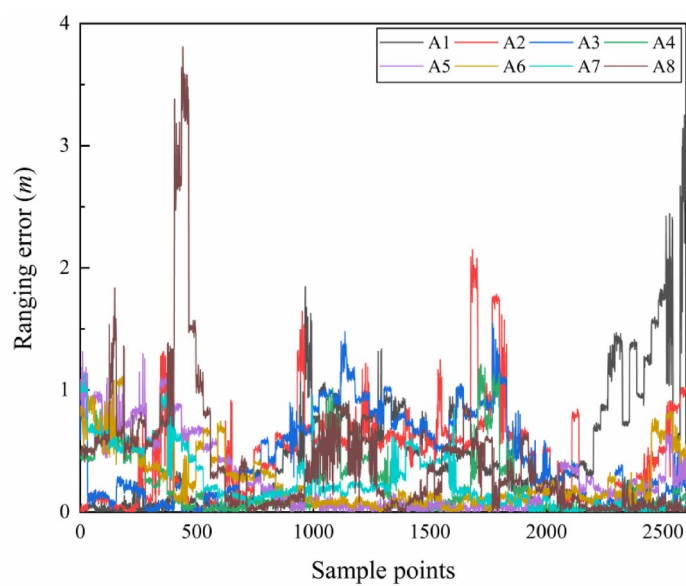
Fig. 6. Ranging error in real world.
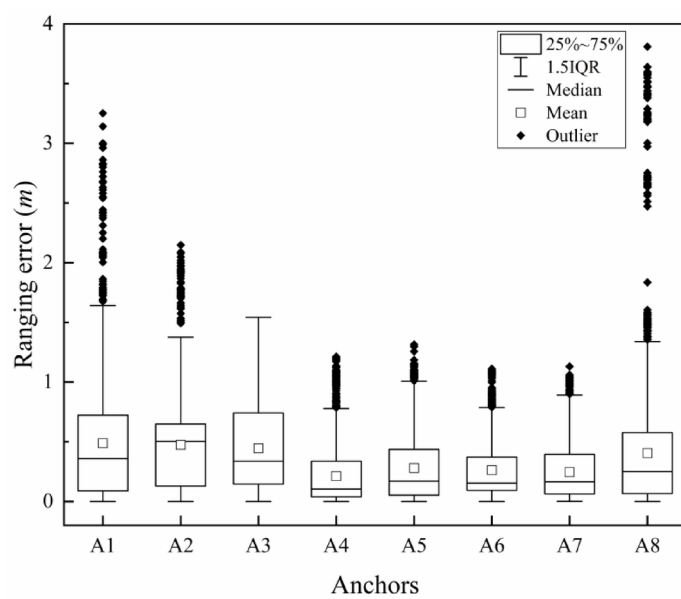
Fig. 7. Boxplot of ranging error.
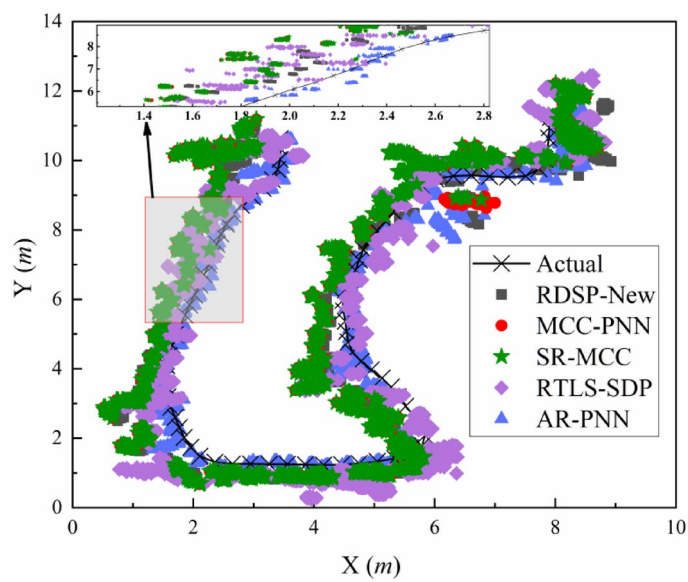
Fig. 8. Comparison of trajectories from different algorithms.
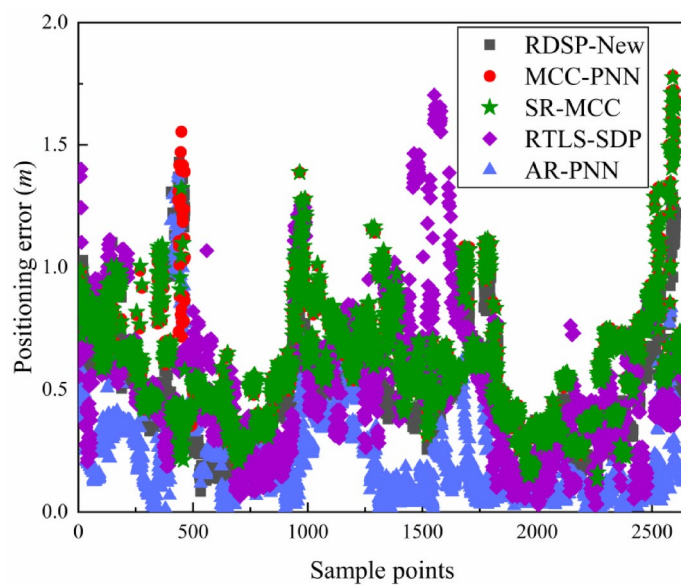
Fig. 9. Comparison of localization errors.
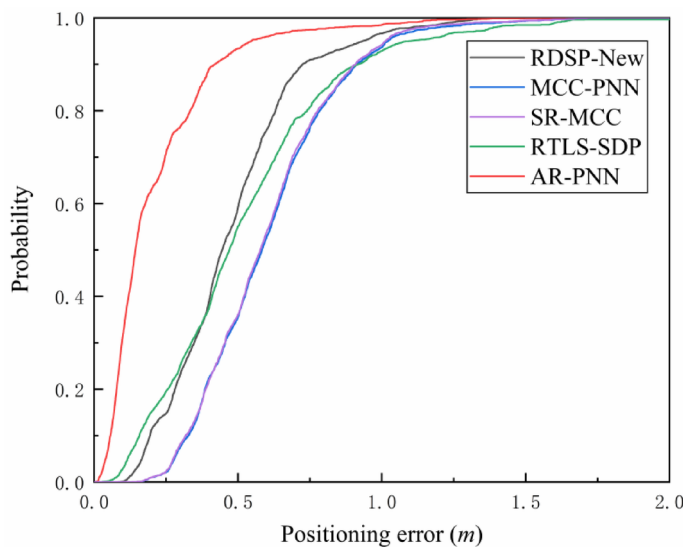
Fig. 10. Comparison of cumulative distribution of positioning errors.

Algorithm	RMSE (m)
SR-MCC	0.37
MCC-PNN	0.38
RDSP-New	0.29
RTLS-SDP	0.35
AR-PNN	0.14

Table 4. Comparison of RMSE localization errors.

Data availability

The datasets used and/or analysed during the current study are available from the corresponding author on reasonable request.

References

1. Isaia, C. & Michaelides, M. P. A review of wireless positioning techniques and technologies: From smart sensors to 6G. *Signals* **4**, 90–136. https://doi.org/10.3390/signals4010006 (2023).
2. Mayer, P., Magno, M. & Benini, L. Self-sustaining ultrawideband positioning system for event-driven indoor localization. *IEEE Internet Things J.* **11**, 1272–1284. https://doi.org/10.1109/JIOT.2023.3289568 (2023).
3. Kapucu, N., & Bilim, M. Internet of Things for Smart Homes and Smart Cities. In *Smart Grid 3.0: Computational and Communication Technologies* 331–356 (Springer International Publishing, Cham, 2023).
4. Deepa, A., Manikandan, N. K., Latha, R., Preetha, J., Kumar, T. S., & Murugan, S. IoT-Based Wearable Devices for Personal Safety and Accident Prevention Systems. In *2023 Second International Conference On Smart Technologies For Smart Nation* 1510–1514 (2023).
5. Nigam, N., Singh, D. P. & Choudhary, J. A review of different components of the intelligent traffic management system (ITMS). *Symmetry* **15**, 583. https://doi.org/10.3390/sym15030583 (2023).
6. Mazhar, F., Khan, M. G. & Sällberg, B. Precise indoor positioning using UWB: A review of methods, algorithms and implementations. *Wirel. Pers. Commun.* **97**, 4467–4491. https://doi.org/10.1007/s11277-017-4734-x (2017).
7. Qi, L., Liu, Y., Yu, Y., Chen, L. & Chen, R. Current status and future trends of meter-level indoor positioning technology: A review. *Remote Sens.* **16**, 398. https://doi.org/10.3390/rs16020398 (2024).
8. Dai, J., Wang, M., Wu, B., Shen, J. & Wang, X. A survey of latest Wi-Fi assisted indoor positioning on different principles. *Sensors* **23**, 7961. https://doi.org/10.3390/s23187961 (2023).
9. Flueratoru, L., Wehrli, S., Magno, M., Lohan, E. S. & Niculescu, D. High-accuracy ranging and localization with ultrawideband communications for energy-constrained devices. *IEEE Internet of Things J.* **9**, 7463–7480. https://doi.org/10.1109/JIOT.2021.3125256 (2021).
10. Mahfouz, M. R., Fathy, A. E., Kuhn, M. J., & Wang, Y. Recent trends and advances in UWB positioning. In *2009 IEEE MTT-S International Microwave Workshop on Wireless Sensing, Local Positioning, and RFID* 1–4 (2009).
11. Wu, H., Liang, L., Mei, X. & Zhang, Y. A convex optimization approach for NLOS error mitigation in TOA-based localization. *IEEE Signal Process. Lett.* **29**, 677–681. https://doi.org/10.1109/LSP.2022.3141938 (2022).
12. Huang, J., & Qian, S. Ultra-wideband indoor localization method based on Kalman filtering and Taylor algorithm. In *3rd International Conference on Internet of Things and Smart City (IoTSC 2023)* 12708, 228–233 (2023).

13. Park, C. H. & Chang, J. H. WLS localization using skipped filter, Hampel filter, bootstrapping and Gaussian mixture EM in LOS/NLOS conditions. *IEEE Access* **7**, 35919–35928. https://doi.org/10.1109/ACCESS.2019.2905367 (2019).
14. He, Y. P. et al. Indoor dynamic object positioning in NLOS environment based on UWB. *Trans. Microsyst. Technol.* **39**, 46–49 (2020).
15. Miramá, V., Bahillo, A., Quintero, V. & Díez, L. E. NLOS detection generated by body shadowing in a 6.5 GHz UWB localization system using machine learning. *IEEE Sens. J.* **23**, 20400–20411 (2023).
16. Singh, S., Trivedi, A. & Saxena, D. Unsupervised LoS/NLoS identification in mmWave communication using two-stage machine learning framework. *Phys. Commun.* **59**, 102118 (2023).
17. Liu, Y. UWB ranging error analysis based on TOA mode. *J. Phys.: Conf. Ser.* **1939**, 012124 (2021).
18. Tomic, S. & Beko, M. A bisection-based approach for exact target localization in NLOS environments. *Signal Process.* **143**, 328–335. https://doi.org/10.1016/j.sigpro.2017.09.019 (2018).
19. Chen, H., Wang, G. & Ansari, N. Improved robust TOA-based localization via NLOS balancing parameter estimation. *IEEE Trans. Veh. Technol.* **68**(6), 6177–6181 (2019).
20. Zheng, R., Wang, G. & Ho, K. C. Accurate semidefinite relaxation method for elliptic localization with unknown transmitter position. *IEEE Trans. Wirel. Commun.* **20**, 2746–2760. https://doi.org/10.1109/TWC.2020.3044217 (2020).
21. Xiong, W., Schindelhauer, C., So, H. C. & Wang, Z. Maximum correntropy criterion for robust TOA-based localization in NLOS environments. *Circuits Syst. Signal Process.* **40**, 6325–6339. https://doi.org/10.1007/s00034-021-01800-y (2021).
22. Xiong, W., Schindelhauer, C., So, H. C., Liang, J., & Wang, Z. Neurodynamic TDOA localization with NLOS mitigation via maximum correntropy criterion. *arXiv preprint* arXiv:2009.06281 (2020).
23. Barron, J. T. A general and adaptive robust loss function. In *Proceedings of the IEEE/CVF conference on computer vision and pattern recognition* 4331–4339 (2019).
24. Singh, S., Trivedi, A. & Saxena, D. Channel estimation for intelligent reflecting surface aided communication via graph transformer. *IEEE Trans. Green Commun. Netw.* **8**, 756–766 (2023).
25. Choi, J. S., Lee, W. H., Lee, J. H., Lee, J. H. & Kim, S. C. Deep learning based NLOS identification with commodity WLAN devices. *IEEE Trans. Veh. Technol.* **67**, 3295–3303 (2017).
26. Che, H. & Wang, J. A collaborative neurodynamic approach to global and combinatorial optimization. *Neural Netw.* **114**, 15–27. https://doi.org/10.1016/j.neunet.2019.02.002 (2019).
27. Hildebrand, F. B. Introduction to numerical analysis. (Courier Corporation, 1987).
28. Bregar, K. Indoor UWB positioning and position tracking data set. *Sci. Data* **10**, 744. https://doi.org/10.1038/s41597-023-02639-5 (2023).

Acknowledgements

Author contributions

Methodology, Y.L.; formal analysis, Y.L.; resources, E.H. and Y.L.; software, Y.L. and E.H.; data curation, C.G. and E.H.; writing—original draft preparation, Y.L.; writing—review and editing, Y.C., C.G. and Y.L.

Declarations

Competing interests

The authors declare no competing interests.

Additional information

Correspondence and requests for materials should be addressed to Y.L.

Reprints and permissions information is available at www.nature.com/reprints.

Publisher's note Springer Nature remains neutral with regard to jurisdictional claims in published maps and institutional affiliations.